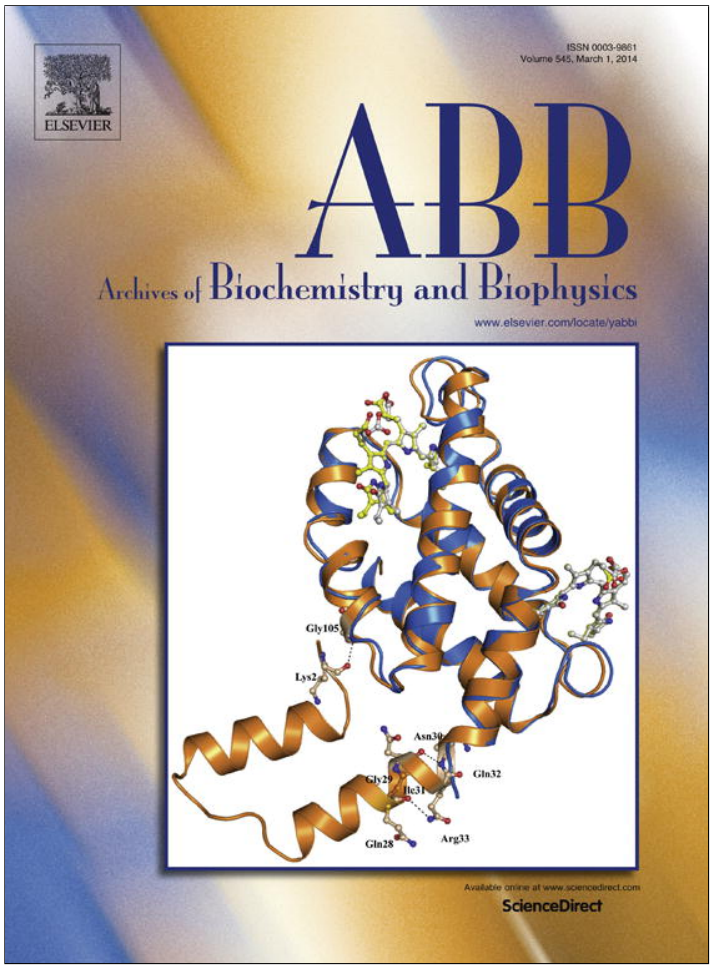

Archives of Biochemistry and Biophysics 545 (2014) 22–32

Contents lists available at ScienceDirect

Archives of Biochemistry and Biophysics

journal homepage: www.elsevier.com/locate/yabbi

Conformational changes involving ammonia tunnel formation and allosteric control in GMP synthetase

Justin C. Oliver [a,1], Ravidra Gudihal [a,2], John W. Burgner [b,3], Anthony M. Pedley [a], Alexander T. Zwierko [c], V. Jo Davisson [a], Rebecca S. Linger [c,*]

[a] Department of Medicinal Chemistry and Molecular Pharmacology, Purdue University, West Lafayette, IN 47907, United States
[b] Bindley Bioscience Center, Purdue University, West Lafayette, IN 47907, United States
[c] Department of Pharmaceutical and Administrative Sciences, University of Charleston, Charleston, WV 25304, United States

ARTICLE INFO

Article history:
Received 19 November 2013
and in revised form 27 December 2013
Available online 13 January 2014

Keywords:
Glutamine amidotransferase
Substrate channeling
Ammonia tunnel
Allosteric control
Conformational change
Purine biosynthesis

ABSTRACT

GMP synthetase is the glutamine amidotransferase that catalyzes the final step in the guanylate branch of *de novo* purine biosynthesis. Conformational changes are required to efficiently couple distal active sites in the protein; however, the nature of these changes has remained elusive. Structural information derived from both limited proteolysis and sedimentation velocity experiments support the hypothesis of nucleotide-induced loop- and domain-closure in the protein. These results were combined with information from sequence conservation and precedents from other glutamine amidotransferases to develop the first structural model of GMPS in a closed, active state. In analyzing this Catalytic model, an interdomain salt bridge was identified residing in the same location as seen in other triad glutamine amidotransferases. Using mutagenesis and kinetic analysis, the salt bridge between H186 and E383 was shown to function as a connection between the two active sites. Mutations at these residues uncoupled the two half-reactions of the enzyme. The chemical events of nucleotide binding initiate a series of conformational changes that culminate in the establishment of a tunnel for ammonia as well as an activated glutaminase catalytic site. The results of this study provide a clearer understanding of the allostery of GMPS, where, for the first time, key substrate binding and interdomain contacts are modeled and analyzed.

Introduction

Guanosine monophosphate synthetase (GMPS)[4] catalyzes the final step in the guanylate branch of purine biosynthesis. In this reaction, the glutamine amide is hydrolyzed and the resulting ammonia is incorporated into xanthosine monophosphate (XMP) to form GMP [1]. Glutamine hydrolysis is achieved by the glutaminase domain, a common protein fold that defines the class I glutamine amidotransferases (GATs) [1]. The glutaminase active site contains a catalytic cysteine (at position 86 in *Escherichia coli* GMPS) and interacts with a histidine and glutamic acid 95 residues downstream [2]. Formation of GMP is achieved in a separate protein domain. A key feature of the class I GATs is tight regulation of glutamine hydrolysis [3]. The glutaminase site is inactive until an acceptor molecule binds and conveys an intramolecular activation signal that stimulates glutamine hydrolysis activity [3–5]. Another distinctive functional component of the amidotransferases is the ability to efficiently achieve interdomain transfer of the nascent ammonia via an intramolecular channel [3,6]. Reviewing the seven class I GAT structures solved to date, [2,7–12] a common face of the glutaminase domain docks to the acceptor domains. In many of these proteins, the docking forms a pathway for ammonia that allows sequestration of this reactive molecule from bulk solvent [6].

As can be deduced by the activity of GMPS, this protein is a metabolically critical enzyme. An adequate supply of cellular nucleotides is critical for nucleic acid production as well as other essential processes of growth and regulation. Cells of the immune system are especially stringent in their requirement of adequate nucleotide pools [13], and targeting the reduction of nucleotide levels in these cells with drugs has been a strategy for immunosuppressive therapies [14–16]. Recent studies of resistance in

* Corresponding author. Address: Department of Pharmaceutical and Administrative Sciences, University of Charleston, 2300 MacCorkle Avenue, SE, Charleston, WV 25304, United States. Fax: +1 304 357 7456.
E-mail address: rebeccalinger@ucwv.edu (R.S. Linger).
[1] Present address: BD Biosciences, 7 Loveton Circle, MC924, Sparks, MD 21152, United States.
[2] Present address: Agilent Life Science Centre India, Block C, Floor 3&4, RMZ Centennial, ITPL Road, Mahadevapura Post, Bangalore 560048, India.
[3] Present address: Virginia Commonwealth University, School of Medicine, Richmond, VA 23298, United States.
[4] *Abbreviations used:* GMPS, Guanosine monophosphate synthetase; XMP, xanthosine monophosphate; GATs, glutamine amidotransferases; L-BFGS, limited-memory Broyden–Fletcher–Goldfarb–Shanno.

0003-9861/$ - see front matter © 2014 Elsevier Inc. All rights reserved.
http://dx.doi.org/10.1016/j.abb.2014.01.004

antimetabolite therapy have revealed a central role for GMPS in the activation of the prodrug thiopurines through similar amination events [17]. Individual resistance to thiopurines has been attributed to genetic polymorphisms in GMPS [18]. GMPS has also been shown to have an allosteric role in the enhanced activation of ubiquitin-specific protease 7, a key enzyme in the regulation of p53 and MDM2 levels [19].

The crystal structure of *E. coli* GMPS [2] provided one of the first views of the two-domain catalytic architecture of a glutamine amidotransferase. The enzyme is a homodimer, with two modular active sites and a third, noncatalytic domain involved in homodimerization. Unfortunately, the six structures of GMPS solved to date have only been captured as catalytically incompetent, with a long, solvent-exposed path between the active sites [2,20–24]. Although ultracentrifugation analysis shows *E. coli* GMPS to exist predominantly as a homodimer in solution [25], all crystallization conditions have yielded an inactive dimer of dimers, with the active sites widely separated and important regions disordered [26], leaving questions of interdomain communication and ammonia transfer unanswered. The problems elicited by the high protein concentrations occurring under crystallization suggest that alternative, solution-based methods may be required to supplement the findings of X-ray crystallography. To this end, NMR studies have recently been performed using the heterodimer of GMPS from the archea bacterium *Methanocaldococcus janaschii*. Isotopic labeling of the glutaminase domain identified interface residues that interact with the synthetase domain [27].

Substrate-induced conformational changes are an important aspect of the activity of many enzyme families, including amidotransferases [28–30]. For example, *E. coli* PRPP amidotransferase contains a large nucleotide-binding loop that becomes ordered upon binding of substrate and forms part of the ammonia channel [31,32]. Molecular dynamics studies showed IGP synthase undergoes a hinging motion upon binding of the nucleotide substrate. This domain motion in turn activated glutamine hydrolysis by reorienting the catalytic triad [33–35]. Further analysis using solution NMR techniques revealed the widespread induction of residue motion in IGP synthase focusing in the hinge region of the protein [36]. However, crystallography studies suggested there may be no subdomain motion in IGP synthase but that nucleotide binding may cause a reorientation of side chains at the subdomain interface 15 Å away that allows glutaminase activation [37].

The solvent-exposed domain organization observed in the six crystal structures of GMPS isoforms suggests that conformational transitions must occur to achieve efficient ammonia transfer. Biochemical evidence suggests that GMPS undergoes structural changes upon substrate binding [38]. Chemical analysis demonstrates that the enzyme adenylates its nucleotide substrate, XMP, after binding [39], and kinetic evidence suggests that ammonia is transferred to the adenylated XMP via an intramolecular path, sequestered from solvent [40,41]. A conserved loop region nucleotide binding site undergoes a disordered-to-ordered transition [2,24]. This 24 amino acid loop had been originally shown to be differentially susceptible to trypsinolysis when exposed to nucleotides [42]. More recently, kinetic and spectroscopic evidence supports a model that implicates coupling of the adenylation reaction and activation of glutaminase through a significant conformational change. [38]. The evidence from both biochemical and crystallographic data support the hypothesis that GMPS must undergo a large, substrate-induced conformational change to establish an intramolecular tunnel for ammonia to traverse the distance between active sites [2].

In the present study, we describe evidence from limited proteolysis, analytical ultracentrifugation, functional analysis of sequence variants, and computational modeling that support a model for a closed catalytically active structure of GMPS. In this closed structure, A conserved loop that was previously disordered in *E. coli* GMPS was modeled using the ordered density from human GMPS with bound substrate. Consistent with a hypothesis for a general allosteric role of interdomain contacts in controlling triad glutamine amidotransferases [34], an interdomain salt bridge between glutaminase residue H186 and synthetase residue E383 was verified in the closed model. The proximity of these two positions at the domain interface and the active sites implicates a functional role that links the XMP active site to the glutaminase active site. For the first time, a model reveals a plausible path taken by ammonia from the glutaminase to the adenylation site in the catalytically competent form of GMPS and establishes a structural basis for the coordinate binding and allosteric effects on the glutaminase active site.

Experimental

Chemicals used in these experiments were of research grade or higher, and water was obtained by purification with a laboratory-grade filtration system. Trypsin (product code TRTPCK) and staphylococcal (V8, product code STAP) protease were obtained from Worthington Biochemicals.

The *E. coli* GMPS used in the analytical ultracentrifugation experiments was obtained by overexpression in *E. coli* according to an existing procedure [43]. For the proteolysis, mass spectrometry and mutagenesis experiments, a simplified method was developed by cloning the full-length GMPS gene into pET28 (Novagen), which imparts an N-terminal polyhistidine tag to the protein. The protein is highly purified by single-step purification through nickel Sepharose (GE Healthcare Life Sciences), and the histidine tag appears to have no detrimental effect on the specific activity or oligomeric state of the protein (data not shown). This tag was not removed before use.

Mutagenesis and expression vector preparation

All site-directed mutagenesis was carried out using Pfu Turbo DNA polymerase with direct mutation in p*guaA*-tac [43]. Sequence confirmation was performed by the Purdue Genomics Core Facility. The mutated gene was then inserted into pET28 using ligation independent cloning. The LIC compatible expression vector pET-L8 was constructed by introduction of ligation-independent cloning sites and addition of TEV protease recognition site after N-term His tag into vector pET30a (Novagen).

The pET-L8 vector was linearized by digestion with Ssp1 restriction enzyme (New England BioLabs), followed by gel purification and then treated with T4 DNA Polymerase (Novagen) in the presence of dGTP (New England Biolab). The reaction was incubated at 22 °C for 30 min, followed by heat inactivation at 75 °C for 20 min.

Forward (5′ TACTTCCAATCCAATGCCATGACGGAAAACATTCAT AAGCATCG) and reverse (5′ TTATCCACTTCCAATGCTATCATTCC CACTCAATGGTAGCTG) primers for guaA inserts were designed and analyzed for compatibility with each other using the program Clone Manager Professional Suite (Scientific and Educational Software, Cary, NC). Inserts for each of the five unique constructs were amplified by PCR from corresponding template plasmids (pguaA Wild Type (WT), pguaA A–A (H 186A/E383A), pguaA E–H (H186E/E383H, pguaA H186A, pguaA E383A) using the high-fidelity polymerase Platinum® *Pfx* DNA Polymerase (Invitrogen). The PCR products were treated with T4 DNA Polymerase in the presence of the dCTP thus generating 5′ overhangs that are complementary to the 3′ overhangs in the linearized and treated vector pET-L8.

To anneal the treated inserts to treated vectors, 0.02 pmol of each insert reaction mix was incubated with 0.01 pmol of vector in 3 μl reaction mix at 22 °C for 10 min. The non-covalent interaction between DNA backbone and insert was stabilized by addition of 1 μL of 25 mM EDTA and incubation at 22 °C for an additional 5 min.

Annealing reactions were directly transformed into X10Gold competent cells (Stratagene) and plated on LB-agar containing Kanamycin (50 μg/ml). Colony PCR analysis was performed to screen for constructs with correct size insert. Plasmids were isolated from selected colonies and verified by sequencing.

Proteolysis and mass spectral analysis

For limited proteolysis of GMPS, protease stocks were made at 1 mg/mL in 1% acetic acid (trypsin) or water (V8). The reactions without nucleotides consisted of 25 mg/mL GMPS in 20 mM buffer (for trypsin, EPPS pH 8.5; for V8, Tris-PO_4, pH 7.8) and 4 mM $MgCl_2$. The nucleotide-containing reactions consisted of the same components, with the addition of 0.25 mM XMP and 1 mM ATP. The reactions were initiated by the addition of protease (4 μg) in a total volume of 100 μL and incubated at 37 °C. Samples were removed at specific time intervals and quenched with the addition of AEBSF to 1 mM and acidification of formic acid to 4%. Standard discontinuous SDS–PAGE gels [44] were run on the samples after neutralization with NaOH and denaturation with loading buffer. Molecular weight estimations and band quantification from gels were performed using ImageJ software [45].

LC/MS experiments were performed with an HPLC (Agilent, model 1100) coupled to an API ion trap mass spectrometer (Bruker Esquire). Separations were performed with 2.1 × 40 mm C8 columns (Higgins Analytical) using gradient elution. Solvent A consisted of 5% acetonitrile and 0.01% TFA in water; solvent B of 0.01% TFA in pure acetonitrile. Elution was achieved by increasing the percentage of solvent B from 0% to 66% over 45 min at 0.2 mL/min. The column was directly attached to the API ionization source of the mass spectrometer, and MS spectra were collected over the entire run. Deconvolution of the spectra were performed either manually with the instrument software or with the use of the program MoWeD [46].

Analytical ultracentrifugation

Sedimentation velocity experiments were performed with a Beckman Optima XL-I analytical ultracentrifuge using the Rayleigh interference optics. Samples with or without nucleotide contained 25 mM EPPS pH 8.5, 125 mM NaCl, 0.5 mM DTT and 1 mg/mL GMPS. Samples with nucleotides also contained 1 mM ATP, 0.5 mM XMP and 4 mM $MgCl_2$, mixed with the protein just prior to the run. Reference solutions were identical to the sample solution except for the presence of protein. Runs were performed at 20° C and 50,000 RPM after an initial 90-min temperature equilibration period. Interference scans were obtained every 30 s for 5 h. The runs were repeated the following day, reversing the sample cells to minimize errors introduced by any rotor asymmetry. SEDFIT was used to generate the necessary files for the program SEPHAT, and each data set was fitted independently using the hybrid fitting algorithm [47].

The sedimentation properties of model GMPS structures were also calculated with a hydrodynamic bead modeling program HYDROPRO, version 7c [48]. The homodimeric form of GMPS was used in these calculations, as this is the predominant quaternary form in solution [25]. Automatic handling of bead radius was used, as was a value of 1.0 cp for solvent viscosity. Solution density was measured with an Anton Paar density meter.

Computational models

Modeling of a closed form of GMPS was accomplished with a combination of software for predicting, manipulating, and minimizing the conformation of protein structures. The closed model was based on the existing crystal structure of the protein, with the addition of the 24-amino acid residue loop that was found to be disordered [2]. This loop, hereafter termed the LID loop, was placed in a random, highly solvent-exposed conformation, with the rest of the protein left unchanged. The secondary structure of the LID loop was predicted using the Robetta server [49] using as a query sequence the residues of the loop and the adjacent 25 residues on either side. Only one result both correctly modeled the structure of the adjacent sequence (as provided by the crystal structure of the protein) and secondary structure for the loop that was sterically compatible with the remainder of the protein. This result was incorporated into the model using the portions adjacent to the LID loop as anchors, leading to an *E. coli* GMPS structure with a complete nucleotide-binding domain, hereafter termed the Catalytic model. Second, the adenylated XMP intermediate was modeled into the nucleotide-binding site of the *E. coli* GMPS based on aspects of the *E. coli* 1GPM crystal structure [2] – including the location of AMP product as well as tetrahedral density that was modeled as belonging to the 5′-phosphate of XMP. Third, since the large-scale motions have been predicted to be involved in the conformational changes of GMPS, manipulation of the domain orientation was also necessary. These changes were accomplished primarily with the use of the program ProteinShop [50], which allowed manual manipulation of sections of the protein.

An assumption guiding this last manipulation was that the primary conformational changes in the protein upon nucleotide binding are experienced by the glutaminase domain. This domain was hinged around the helix marking the end of the domain (residues 210–225) to move it closer to the nucleotide-binding domain. Finally, the structure was energy minimized using Sybyl 7.0 (Tripos, Inc.). For the Catalytic model, cavity analysis and visualization were performed with the programs Voidoo/Flood [51] and CASTp [52]. The probe radius used in the calculations was 1.5–2.0 Å.

Sequence alignments

GMPS sequences were aligned using the sequence alignment program ClustalW (version 1.83) [53] as implemented in the program Bioedit (version 7.0.5.3) [54]. Analysis of conservation of the GMPS sequence was performed with the ConSurf server [55], using the default options for version 3.0 of the software, except for the value of the maximum number of homologues to be considered in the analysis, which was increased from 50 to the entire set of sequences with PSI-BLAST [56] *E*-values below a cutoff of 0.001. Since amidotransferases consist of modular domains [3], each domain was considered separately in the conservation analysis.

Kinetic and stoichiometric assays

Glutamine-dependent synthetase assays were performed as previously described [57]. Steady-state kinetic assays of GMPS in the presence of ammonium were performed using the conditions described in the glutamine-dependent assays with the substitution of 200 mM ammonium chloride for glutamine. Steady-state kinetics studies of the glutaminase half-reaction or stimulated glutaminase and basal glutaminase activity were performed using a 96-well plate format. The initial reactions were built with a final volume of 100 μL in 96-well PCR plates with each well containing 0.1 M EPPS, pH 8.5, 20 mM $MgCl_2$, 2.5 mM EDTA, 0.1 mM DTT, 2 mM ATP, 200 μM XMP and varying concentrations of glutamine (eight replicates each). GMPS amounts used varied depending on

the activity of the mutant. The remaining wells were used to establish a glutamic acid standard curve. The plate was incubated at 37 °C with 200 RPM shaking for 15 min and the reaction was quenched by placing the plate into a 110 °C sand bath for 1 min. Analysis of formed glutamic acid proceeded as previously described [58]. Basal glutaminase assays differed from the above as follows: water replaced XMP, and the wells containing varying concentrations of glutamine were split such that four did not contain GMPS, while the other four were incubated with the enzyme. This allowed subtraction of contaminating glutamic acid in the glutamine stock solution from the results of each glutamine concentration. Analyses of the reaction stoichiometry were performed as end point assays. To assess GMP formation, we followed the protocol established by Sakamoto [59], a reaction containing 100 mM EPPS, pH 8.5, 1 mM EDTA, 100 μM DTT, 20 mM $MgCl_2$, 2 mM ATP, 200 μM XMP and 20 mM glutamine were incubated for 5 min. The reaction was quenched by the addition of 70% perchloric acid to a final concentration of 3.15%. The absorbance of the quenched reaction was measured at 290 nm using an extinction coefficient of $6 \times 10^3\ M^{-1}\ cm^{-1}$ for GMP. Background subtraction was achieved with a duplicate reaction excluding XMP. Glutamic acid formation was measured using the glutamate dehydrogenase coupled reaction analysis, where reaction mixtures, as described above, were incubated and quenched by boiling in a 110 °C sand bath for three min., with analysis proceeding as previously described [58].

Results

Limited proteolysis

Limited proteolysis methods have been used to probe for regions of disorder in proteins, including loops [60,61]. As an approach to probe the structural regions involved in the conformational changes in GMPS upon binding of substrates, limited digestion of the enzyme with trypsin or staphylococcal (V8) protease was performed in the presence or absence of substrate nucleotides, XMP and ATP, plus magnesium. Using the crystal structure data, the substrate specificity of trypsin (arginine and lysine) and V8 protease (aspartate and glutamate) and higher resolution mapping of the cleavage sites under limited conditions provided a structural basis for analysis of the conformational states. The qualitative protection of GMPS from trypsinolysis by substrates has been observed previously. [42], while the findings with V8 protease are reported here. Reverse-phase LC/MS analysis of the limited proteolysis reactions was used to reveal the exact positions of the differential cleavage. Although a number of bands observed in SDS–PAGE were not detected in the LC/MS experiments, key fragments were identified, and was consistent with the conformational model proposed.

A difference in proteolytic susceptibility between the nucleotide-bound and free states was evident from SDS–PAGE analysis of the time dependent proteolytic reaction samples (Fig. 1). Quantification by densitometry of the band for the intact GMPS protein in the trypsin reaction gel also showed an effective stabilization by the addition of nucleotide substrates (Fig. S1). A linear least-squares regression curve fit through the log of these data points indicates that the rate of disappearance of the nucleotide-bound form of the enzyme was nearly 10 times more stable against proteolysis than the unliganded form of the protein.

The clearest indication of the conformational differences induced in GMPS by nucleotides arose from the trypsinolysis reactions. The major protein fragments of GMPS from these experiments separated and analyzed by LC/MS had molecular weights of 19,805, 19,256 and 18,229 Da. The corresponding cleavage sites occur in the C-terminal region of GMPS after lysine

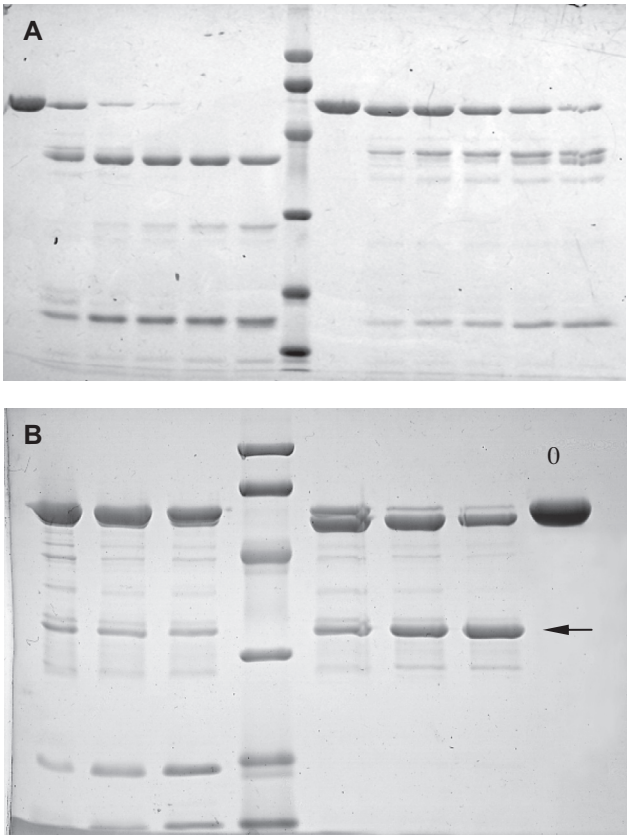

Fig. 1. Differential proteolysis of GMPS in the presence or absence of nucleotides. Gel A shows time points from cleavage of the protein with trypsin; gel B with staphylococcal (V8) protease. MW of ladder bands: 97.4, 66, 45, 31, 21.5 and 14.4 kDa. In both gels, the group of lanes to the left of the molecular weight ladder shows time points from the reactions without substrate, while the group to the right shows the same time points from reactions with substrate. Time points in gel A (left to right): 0, 1, 3, 5, 10, 20 min. Time points in gel B (left to right): 5, 15, 30 min, with lane marked "0" showing uncut protein. Arrow in gel B indicates the "core fragment" (see text).

residues 351, 356 and 366 in the LID loop (Fig. S2). Deconvolution of the LC/MS profiles for these three fragments allowed for their quantification in the reactions as a function of time, and the results are shown in (Fig. S3). Importantly, the fragments arising from cleavage at lysine residues 351 and 356 appeared to increase in abundance at the early time interval under conditions where no nucleotides were present (Fig. S3a and b). The presence of nucleotide led to the reduction in cleavage at these sites over the same time period. In contrast, there was little difference in the apparent rate of cleavage at K366 as a function of the substrate nucleotide (Fig. S3c). The abundance of the resulting 18229 Da fragment was less at each time point when nucleotides were present, consistent with a reduction in the rate of cleavage at K366 when nucleotide was present.

A comparative analysis was pursued using a protease of different substrate specificity. Fig. S3d shows the results of the time course of GMPS cleavage by V8 protease. Distinct differences in the banding patterns were observed depending upon the presence or absence of nucleotide substrates. A band in the V8 gel appeared to accumulate in the reactions with nucleotide only present at relatively low and unchanging levels in the absence of substrates (Fig. 1, arrow). Secondary cleavage products are observed at lower molecular weights. Image analysis [45] of the gel band at 36 kDa was consistent with the LC/MS analysis of these digests, which revealed a fragment of mass 35709 Da (data not shown). This fragment was attributed to a portion of the protein (termed the

"core fragment") between the V8 cleavage sites at glutamate residues 66 and 390 (Fig. S3). While trypsinolysis demonstrated the effect of loop ordering by nucleotide binding, V8 proteolysis demonstrated the possibility for whole-domain motions leading to a compact, protease-resistant GMPS structure. This result was consistent with the resistance to nonspecific proteases or heat inactivation reported earlier [42]. In the presence of nucleotides, the core fragment appeared to remain intact and accumulate even after liberation by V8 cleavage at glutamic acids 66 and 390 (Fig. S3d). However, in the absence of nucleotides, the interdomain association appeared diminished, as demonstrated by the lack of accumulation of the core fragment and the presence of lower molecular weight bands in the lanes without nucleotide (Fig. 1B).

Sedimentation velocity

Sedimentation velocity experiments were performed in duplicate on GMPS in the presence or absence of nucleotide substrates. Apart from nucleotides, the solvent conditions were carefully matched between the two experiments to allow an assessment of sedimentation differences between the two states at an accuracy of +/−0.1% for such side by side comparisons in the same run [62,63]. Substrate nucleotides appeared to induce a reproducible 0.3 S difference in the sedimentation of GMPS (Table 1). Since only an approximately 0.07 S increase in sedimentation was predicted from the increase in mass imparted by binding of ATP and XMP substrates alone, without any conformational change (Table 1), the measured increase in *S*-value implied that the structure becomes more compact upon binding, giving rise to increased sedimentation rate. Moreover, the two major predicted aspects of the GMPS conformational change, loop ordering and domain motion, both appeared to be necessary to achieve the increase in sedimentation rate observed after mixing protein with nucleotide substrates (Table 1).

Molecular modeling of a closed structure

The crystal structure of *E. coli* GMPS pdb: 1gpm (Fig. 2a) is incomplete for a region of high sequence conservation (Fig. S4) at residues 344–368 (called the LID loop). The proximity of this loop region to the ATP binding site [2] implicates a functional role in substrate binding. Before any modeling of the missing density could be undertaken, certain protein-substrate interactions needed to be modeled. The crystal structure contained density for AMP in the nucleotide binding domain and this density served as the starting point to create an adenylated XMP intermediate bound in the active site of the synthetase domain. In addition, the protein crystalized in a largely solvent exposed conformation, with the subdomain interfaces several angstroms from each other. Large scale domain motions have been predicted for GMPS The glutaminase domain was therefore manually reoriented such that the glutaminase active-site docked against the nucleotide binding domain, creating an interdomain chamber similar to what is seen in other amidotransferase structures.

An important constraint for modeling the missing loop density is the resistance of the LID loop to trypsinolysis upon nucleotide binding. Since the loop contains several trypsin cleavage sites that would be highly accessible in the open form, a disorder-to-order transition of this loop is very likely to occur upon nucleotide binding, as seen in the human GMPS structure. Secondary structure for the LID loop was predicted using the Robetta server. Twenty-five crystalized residues on either side of the missing density were included to help verify the model. The model was chosen that showed those residues correctly modeled to reflect their crystalized secondary structure along with sterically compatible density for the LID loop.

The Robetta model generated for the LID loop is supported by the trypsinolysis data reported above. The two trypsin sites that are observed to be protected by nucleotide from cleavage, K351 and K356, are potentially involved in interactions with the substrate, while the third, unprotected site, K366, is not (Fig. S5). The model was then subjected to a molecular dynamics simulations resulting in an energy minimized closed GMPS model (Fig. 2B).

A second closed model

After the Robetta structure prediction model was created, a crystal structure of the human isoform of GMPS with density corresponding to the LID loop (*E. coli* numbering) was released (2VXO). Although the model was consistent with the trypsinolysis results, the critical role for the loop structure warranted further consideration. A model of the closed structure using this human isoform LID loop density was created (see supplemental data for method). In minimizing the model, however, a different force field algorithm was used (limited-memory Broyden–Fletcher–Goldfarb–Shanno (L-BFGS) algorithm in Desmond) (Fig. 2C).

Comparing this second model with the Catalytic model just described, there are significant differences in LID loop interactions with the homodimer-binding domain (Fig. 3). As a result, the homodimer-binding domain of GMPS is seen to be drawn away from the XMP binding site exposing the active site and interface domain to bulk solvent as if in product release. Henceforth, this model will be termed the Release model (Fig. 3).

Computational analyses of the models

Intramolecular ammonia channeling is a recurring theme in amidotransferases, and these channels are consistently lined with residues that are conserved and largely hydrophobic [9,64–67]. The Catalytic model of GMPS satisfied these requirements. The domain closure brought the glutaminase active-site cysteine nearer to the nucleotide binding domain by approximately 13 Å while also establishing an ammonia path. Analysis with Voidoo [51] and CASTp [52] revealed a large, essentially solvent-excluded cavity (termed the ammonia tunnel) between the adenylated XMP intermediate and the cysteine active site residue of the glutaminase in the Catalytic model structure (Fig. 4A). When a 2 Å probe radius was used, no exits from this cavity to the surrounding

Table 1
Sedimentation values predicted by HYDROPRO for the models of free (open model) and nucleotide-bound GMPS (closed model). The rows in italics are from experimental data, not HYDROPRO predictions.

Model	Mass used in calculation (Da)	Sedimentation (*S*)
(*GMPS without nucleotides*)	–	*5.67* (*observed*)
Catalytic model with open glutaminase (closed 344–368 loop)	119130	5.78
Catalytic model with open 344–368 loop (closed glutaminase)	119130	5.88
Catalytic model (both loop and glutaminase closed)	119130	5.94
(*GMPS + XMP + ATP*)	–	*5.96* (*observed*)

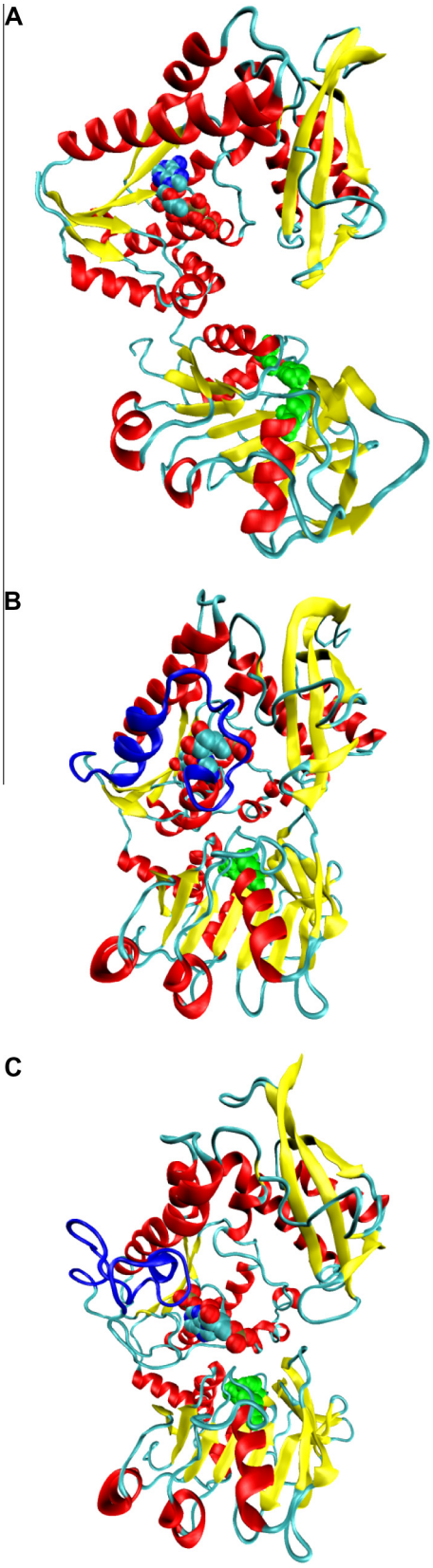

Fig. 2. (A) 1GPM crystal structure, with AMP and pyrophosphate modeled in spacefill. (B) Catalytic model with Adenylyl-XMP in spacefill, LID loop in blue. (C) Release model with Adenylyl-XMP in spacefill, LID loop in blue. All models show glutaminase catalytic triad in green spacefill. (For interpretation of the references to color in this figure legend, the reader is referred to the web version of this article.)

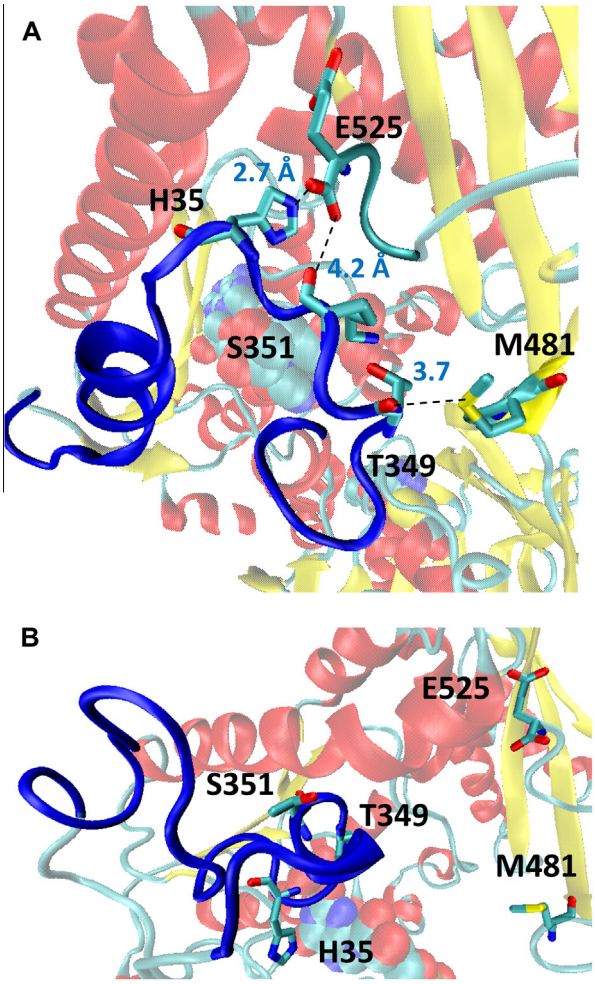

Fig. 3. (A) Catalytic model showing LID loop interactions (T349, S351 and H353) with dimer-domain residues (M481 and E525). (B) Release model showing no interactions between the LID loop and the dimer-domain interface.

solvent were found; however when the probe was reduced to 1.5 Å, a small number of exits were found, but they were distal to the path between the glutaminase active site and the nucleotide intermediate (data not shown).

With the Release model, Voidoo and CASTp analyses showed that the ammonia tunnel, including the interior of the nucleotide binding site was now solvent exposed (Fig. 4B), with the nucleotide exiting the active site. These results support the model as showing product release. Consurf [55] conservation scores of the ammonia tunnel-lining residues were high (Fig. 4A); the residues facing the tunnel had a propensity toward a hydrophobic or non-polar nature, with the exception of the highly conserved residues that may be involved in nucleotide binding.

The V8 protease digest data supported the closed nature of the Catalytic model (Fig. 2B) When nucleotides were present in the digests, the model positions the glutaminase domain closer to the nucleotide-binding domain, while in the open, unbound form, the glutaminase is more mobile and distant from the synthetase domain. On average, an open form would display more proteolysis sites. The lower molecular weight of the proteolysis product bands in the V8 gel (Fig. 1) is consistent with greater susceptibility to cleavage. In contrast, although V8 appeared to rapidly cut at two distal loops in the closed, nucleotide-bound enzyme, the remaining fragment remained resistant to further cleavage, likely due to the stabilization of a closed, compact conformation.

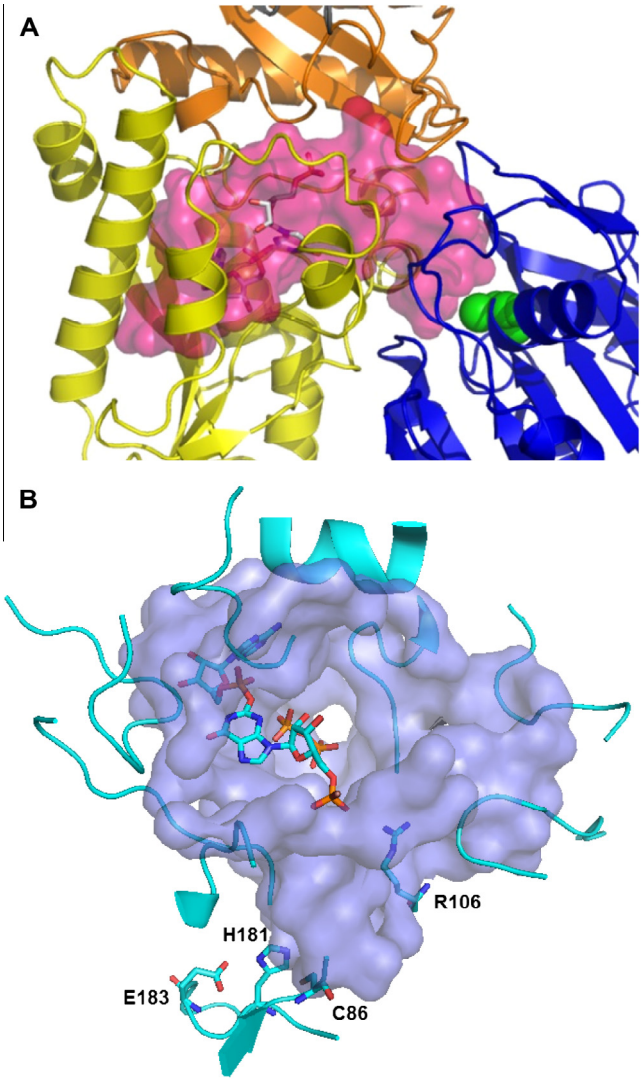

Fig. 4. Proposed GMPS ammonia tunnel and conservation of tunnel residues in both models. (A) Catalytic model. Interdomain ammonia tunnel in pink. Highly conserved residues (ones with a Consurf conservation index of 7–9 out of 9) are colored yellow. (B) Release model. Surface of solvent exposed interdomain ammonia tunnel in gray. Adenylyl-XMP intermediate and catalytic triad residues in licorice. (For interpretation of the references to color in this figure legend, the reader is referred to the web version of this article.)

A final constraint on the Catalytic model came from the data provided by the differential sedimentation velocity experiments. The difference in sedimentation values seen in these experiments provided a basis for evaluation of the overall structure of the Catalytic model. Bead modeling software (HYDROPRO) allowed the calculation of hydrodynamic properties based on model structures to refine and corroborate the structural predictions for GMPS. The enzyme was observed to be a homodimer in solution [25], and the *S*-values of the closed homodimer model structures (Catalytic model) as given by bead modeling corresponded closely with the values seen in the experiment (Table 1).

Probing the role of the interdomain salt bridge in the allosteric control of the glutaminase active site

The glutaminase active site resides at the interface of the two subdomains in GMPS. In the closed model, a salt bridge was formed between H186 in the glutaminase domain and E383 in the synthetase domain (Fig. 5). Histidine 186 is two residues from the

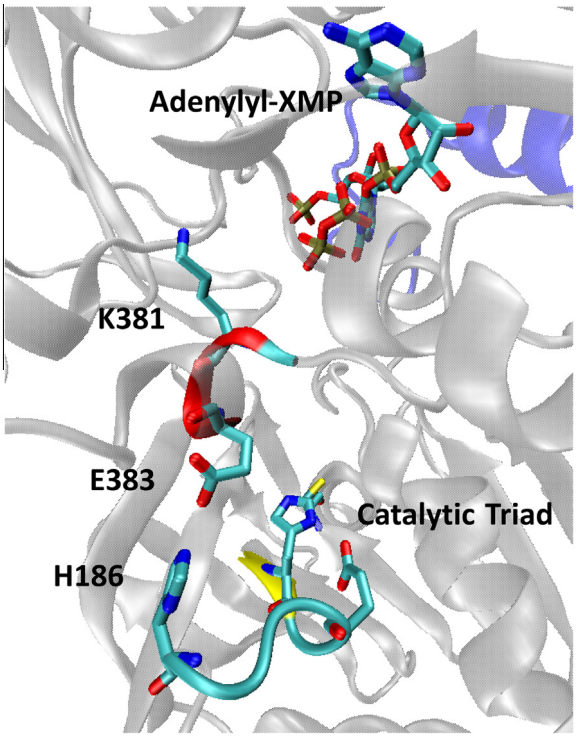

Fig. 5. Catalytic model showing interdomain contacts between the glutaminase catalytic triad and K181, which extends into the ATP binding site of the synthetase domain.

glutamic acid (E183) of the catalytic triad in the glutaminase active site. The glutaminase domain is highly conserved in all triad glutamine amidotransferases. Histidine 186 is in the same location as K196 identified in IGP synthase, a residue which has been shown to contribute a key interdomain contact conferring the acceptor substrate binding signal to the glutaminase active site through ionic interaction with a charged residue from the acceptor domain [34]. Similar contacts were identified in the crystal structures of CTP synthetase, FGAR-amidotransferase and anthranilate synthase [34].

E383: the synthetase component of the interdomain salt bridge

Mutation of E383 to alanine disrupted the capacity of XMP to signal glutaminase activity by eightfold (Table 2), with a threefold reduction in XMP turnover. Stoichiometric analysis of this mutant indicated a moderate uncoupling (2:1) of the two reactions (Table 2). The alanine mutation still allowed basal glutaminase activity as seen by the altered stoichiometry of two glutamine hydrolytic events to one XMP turnover. This result suggests that competency of the glutamine active site in the absence of XMP is enhanced, without disrupting the ammonia transfer.

H186: the interacting residue adjacent to the glutaminase catalytic triad

The H186 residue proximal to the glutaminase active site in the closed model bridges to the acceptor domain through interactions with E383. Mutation to alanine disrupted the K_m for glutamine by 50-fold and 34-fold. Any impact upon XMP turnover kinetics was not observed. As with wild type, there was no detectable glutamine turnover in the absence of XMP. The differences in the catalytic efficiency for the glutaminase half-reaction and XMP turnover are consistent with an uncoupling of the two functions (Table 2)

Table 2
GMPS Kinetic Parameters.

E. coli GMPS Synthetase Kinetic Parameters

Mutation	K_m, XMP(Gln) (μM)	k_{cat} (s^{-1})	k_{cat}/K_m(M^{-1} s^{-1}) ($\times 10^5$)	k_{cat}/K_m wt/mut	K_m, XMP(NH_4^+) (μM)	k_{cat} (s^{-1})	k_{cat}/K_m(M^{-1} s^{-1}) ($\times 10^5$)	k_{cat}/K_m wt/mut	K_m, Gln(mM)	k_{cat} (s^{-1})	k_{cat}/K_m (M^{-1} s^{-1})	k_{cat}/K_m wt/mut
Wild type	53 ± 7	23 ± 1	$4.3 \pm 0.6 \times 10^5$		43 ± 4	13.3 ± 0.3	$3.1 \pm 0.3 \times 10^5$		1.6 ± 0.3	13.7 ± 0.5	$8 \pm 1 \times 10^3$	
H186A	45 ± 10	14 ± 2	$3.1 \pm 0.9 \times 10^5$	1	50 ± 6	15.6 ± 0.8	$3.1 \pm 0.4 \times 10^5$	1	80 ± 10	16 ± 1	$2.1 \pm 0.4 \times 10^2$	38
E383A	22 ± 3	3.2 ± 0.2	$1.4 \pm 0.2 \times 10^5$	3	56 ± 7	7.0 ± 0.3	$1.2 \pm 0.2 \times 10^5$	3	3.2 ± 0.4	3.2 ± 0.1	$1.0 \pm 0.2 \times 10^3$	8
H186A/E383A	7 ± 2	0.85 ± 0.04	$1.1 \pm 0.3 \times 10^5$	4	74 ± 7	9.0 ± 0.3	$1.2 \pm 0.1 \times 10^5$	3	99 ± 12	4.8 ± 0.3	49 ± 7	163
H186E/E383H	8 ± 1	0.81 ± 0.03	$1.0 \pm 0.2 \times 10^5$	4	50 ± 10	6.1 ± 0.4	$1.2 \pm 0.3 \times 10^5$	3	67 ± 9	4.7 ± 0.3	$7 \pm 1 \times 10^1$	114

E. coli GMPS Glutaminase Kinetic Parameters

Mutation	K_m, Basal, Gln (mM)	k_{cat} (s^{-1})	k_{cat}/K_m (M^{-1} s^{-1})	K_m, 1/2 Rxn, Gln (mM)	k_{cat} (s^{-1})	k_{cat}/K_m (M^{-1} s^{-1})	k_{cat}/K_m wt/mut	k_{cat}/K_m stim/basal	Stoichiometry Glu/GMP
Wild type	n.d.*	n.d.	n.d.	1.75 ± 0.06	29.3 ± 0.3	$1.67 \pm 0.06 \times 10^4$			1:1
H186A	n.d.	n.d.	n.d.	60 ± 10	5.2 ± 0.5	$8 \pm 2 \times 10^1$	209		8:1
E383A	$1.4 \pm 0.4 \times 10^2$	$2.0 \pm 0.3 \times 10^{-3}$	$15 \pm 5 \times 10^{-3}$	2.7 ± 0.3	5.5 ± .2	$2.0 \pm 0.3 \times 10^3$	8	136.600	2:1
H186A/E383A	$1.3 \pm 0.2 \times 10^2$	$5 \pm 0.4 \times 10^{-3}$	$41 \pm 6 \times 10^{-3}$	70 ± 20	5.3 ± 0.7	$7 \pm 2 \times 10^1$	239	3.700	15:1
H186E/E383H	$1.7 \pm 0.6 \times 10^2$	$8 \pm 2 \times 10^{-3}$	$5 \pm 2 \times 10^{-2}$	46 ± 7	7.0 ± 0.5	$15 \pm 3 \times 10^1$	111	7.100	26:1

* Not detectable.

as is seen with the 8:1 stoichiometry glutamine hydrolytic events to XMP turnover (Table 2).

H186A/E383A: removing the interdomain salt bridge

To probe the effect of the interdomain salt bridge on the coupling of the two reactions, both residues were mutated to alanine to remove any possibility of non-specific interaction between the two subdomains by these residues. Of all the mutants, H186A/E383A exhibited poor solubility (data not shown). As anticipated, the glutaminase catalytic efficiency was significantly disrupted by 163-fold and 239-fold (Table 2). Basal glutaminase activity was detectable with the H186A/E383A double mutant; however, the degree of disruption of the K_m for glutamine (130 mM, Table 2) prevented assays under condition of full saturation, due to limits of the solubility of the glutamine substrate. XMP turnover in this mutant was only slightly disrupted, with a threefold reduction in the catalytic efficiency. Stoichiometric analysis revealed a significant uncoupling of the two reactions with 15:1 glutamine/XMP turnover (Table 2).

H186E/E383H: inverting the interdomain salt bridge

Finally, a "switch" mutant was created, where the amino acids of the interdomain salt bridge were interchanged. If these residues were interacting with only each other, then it was hypothesized this "switch" mutation would have similar kinetics to wild type. Significant disruption in the glutaminase activities for this mutant were observed by 114-fold and 111-fold changes in catalytic efficiency, while the XMP turnover remained relatively unchanged (Table 2). There was detectable basal glutaminase activity; however, the increased glutamine K_m again did not allow for full saturation of the enzyme. The stoichiometry of the reactions for this mutant was 26:1, indicating significant uncoupling of the two half-reactions (Table 2). The fact that the results for this mutant were not similar to wild type indicates that these "switched" residues may have additional interactions within the protein structure that are greatly disrupted by changing the electrostatic nature of the amino acid. Taken together, the lines of evidence presented above all support the Catalytic model proposed here showing the active, closed form of GMPS.

Discussion

The X-ray crystal structure of GMPS provided the first detailed view for both the triad-type glutaminase and N-type pyrophosphatase enzyme classes [2], and this structure was one of the earliest in the broader class of glutamine amidotransferases. However, the data represented an inactive, product-bound form. Key details in the function the enzyme were not directly addressed, including the path of ammonia during catalysis and the binding site of XMP substrate. Six additional structures of GMPS have been solved, and all show the protein in a catalytically unfavorable, solvent exposed conformation [2,20–24]. The results presented here provide the basis for a closed, active enzyme form that addresses some of these remaining questions.

A pathway for ammonia

An important precedent for the modeling of a closed GMPS was the crystal structure of a closed form of *E. coli* GPATase bound to a non-hydrolyzable substrate analog [31,64]. In this amidotransferase, a large loop orders upon binding its nucleotide substrate and thereby generates a transient, solvent-excluded tunnel for ammonia. The path taken by ammonia in GPATase is lined with conserved, hydrophobic or nonpolar residues, and ionic or polar interactions are involved in the binding of a nucleotide substrate at one end of the tunnel. In the closed model (Catalytic model) of GMPS, a very similar picture of enzyme function is seen, with a transient, solvent-excluded path being generated by the ordering of a substrate-binding loop and by hinging motions of the glutaminase domain toward the nucleotide-binding domain. Also similar to GPATase, the conservation of the proposed tunnel-lining residues is also high in the GMPS model, with a predominance of weakly interacting residues that would not impede the transmission of ammonia between active sites via hydrogen bonding. Water is thereby excluded from the path in both enzymes by the hydrophobic character of the tunnels which would favor the transfer of ammonia and not ammonium ion. Several GAT structures indicate flexible loops, or subdomain motions that help to shield the glutaminase active site upon ligand binding and create an ammonia tunnel within the protein [68–70]. For example, in 2-amino-2-desoxyisochorismate synthase, the binding of the substrate chorismic acid causes subdomain motions that form a 25 Å ammonia tunnel between the glutaminase and acceptor active sites [71].

An additional section of the proposed ammonia tunnel is defined by the LID loop of the GMPS synthetase domain. While this loop was disordered in *E. coli* GMPS (1GPM), it was ordered in the human isoform crystal structure. The Catalytic model predicted secondary structure elements for this loop and modeled the loop

into the closed version of the enzyme creating key protein contacts between the loop and the homodimer binding region, where two molecules of GMPS interact (Fig. 3A). With the Release model, the random loop was defined using density from the human isoform of GMPS, which crystallized in an open form, and since no intramolecular contacts were defined for the loop, the homodimer binding region appears slightly open and more solvent exposed than the Catalytic model.

The Catalytic model for the closed form of GMPS reinforces the idea proposed earlier [64] regarding the apparent dichotomy in amidotransferase ammonia tunneling. The enzymes that generate a channel during each cycle with a conformational change require a lining of hydrophobic and nonpolar residues to minimize the presence of water in the ammonia tunnel, which could lead to inefficient hydrolysis of substrates. In contrast, proteins with preformed ammonia tunnels, such as carbamoyl phosphate synthetase [66], tend to have a reduced requirement for such hydrophobicity and may have other mechanisms in place to minimize the interference of water. Evidence of loop closure is seen in the trypsinolysis data. Domain motion and an increase in compactness are suggested by the V8 protease data, and generated computational models reflect the sedimentation velocity data and provide constraints for all proposed conformational changes in the models.

XMP binding site

In the Catalytic model for the closed structure of GMPS, highly conserved residues within the LID loop (Fig. S4) are in juxtaposition to the adenylated XMP (Fig. 2B). Proteolysis experiments with this protein indicates that the LID loop is protected from proteolytic cleavage when nucleotide is bound, suggesting the LID loop participates in substrate binding. Given the fact that this region is highly conserved in GMP synthetase, it is proposed that the LID loop may participate in substrate recognition. With the Catalytic Model, this study suggests that the loop may participate in the communication between the active sites and facilitate ammonia transfer as the LID loop creates a wall of the putative ammonia tunnel in the interdomain region.

The role of the interdomain salt bridge in glutaminase activation

In the closed model, a salt bridge between H186 in the glutaminase domain and E383 on the acceptor domain makes up the outer edge of the ammonia cavity and mutations at these residues may allow bulk solvent access to the chamber. Both members of this salt bridge are found in highly conserved regions of the protein that include residues in each active site. H186 resides in the same location on the glutaminase domain as charged amino acids interacting in interdomain salt bridges identified in other triad glutamine amidotransferases (Table 3). Analysis of the roles of these charged residues in the coupling of the two half-reactions was pursued in IGP synthase, where K196 was mutated and analyzed in turnover kinetics [34] suggesting that K196 forms a key interaction between the subdomains and confers a signal upon acceptor substrate binding to the catalytic triad. In addition, K196 was seen to play a role in the competency of the glutaminase active site to adequately bind glutamine.

In a recent NMR study of the GMPS glutaminase domain, H186 (H168 in *M. jannaschii*) was identified as directly interacting with the ATPase domain [27]. Mutation of H186 and E383 in *E. coli* GMPS resulted in uncoupling of the two half-reactions of the enzyme; however, the degree of disruption (Table 2) indicated that the resulting ammonia may not be completely lost from the interdomain chamber as seen in similar studies with IGP synthase [34]. Mutations at H186 significantly altered the kinetic constants for glutamine in both synthetase and glutaminase half-reactions. Histidine 186 appears to act as a stabilizer of the glutaminase active site, and helps to orient the histidine (H181) and glutamic acid (E183) of the catalytic triad into a catalytically optimal conformation. Conversely, mutations at E383 resulted in moderate disruptions of the two half-reactions. As confirmed with the double mutant, as long as H186 remained intact, the binding signal could still be conferred to the glutaminase active site. Mutations at E383 allowed detectable basal glutaminase activity and indicate a role for this residue in the regulation of glutamine hydrolysis. In this study, only mutants with changes at this position allowed basal glutaminase activity, though E383A only moderately disrupted the glutaminase half-reaction. Adjacent to E383 is the highly conserved D382, which could interact with H186 in the E383A mutation. The side chain of D382 is within 7 Å of H186 in the model structure, and a slight shift of the random loop containing H186 may allow a compensating interaction with D382. Both E383 and D382 reside in a highly conserved region of the protein that begins with K381, which interacts with the pyrophosphate fragment from ATP in the crystal structure of *E. coli* GMPS (1GPM). A direct linkage to the nucleotide binding site with E383 is observed through this backbone connection (Fig. 5).

Mechanism of glutaminase signaling in GMPS

Loops in the vicinity of the active site cysteine of the triad glutaminases may play a general role in modulating the glutamine hydrolysis activity [68]. The loop in GMPS that gives rise to the oxyanion hole appears to be in a favorable conformation, with the backbone nitrogen of G59 and Y87 positioned to interact with the negative oxyanion of the transition state [2]. These observations led to the hypothesis that the glutamine hydrolytic machinery is poised to perform catalysis, but full glutaminase activity is only achieved by formation of a complete binding site for glutamine [2].

Inspection of the glutamine binding pocket in the crystal structure of GMPS shows three loops that may be involved in modulation of glutaminase activity, one that provides part of the oxyanion hole (loop 1, residues 59–65), a second that lies on the opposite side of the glutamine binding cleft (loop 2, residues 142–147), and a third that lies more external to the other loops (loop 3, residues 100–108) (Fig. 6). Comparison of the GMPS structure with that of the CPS glutamyl thioester adduct [7] reveals possibilities for loop motions that may be required to form a complete glutamine binding site and stimulate glutaminase activity. One possible motion is the orientation of loop 2, which would not provide optimum hydrogen bonding interactions with the alpha-carboxyl portion of glutamine. Another feature could involve an interaction between loops 1 and 3. In the *E. coli* GMPS crystal structure, an arginine in loop 3 (R106) is involved in hydrogen bonds with the backbone oxygens of P60 and E61 of loop 1, which may "cover" the glutamine binding site and preclude substrate from binding.

Conformational changes originating in the acceptor domain may also cause shifts of these loops, allowing activation of glutaminase binding site. In the Catalytic model for GMPS, the acceptor domain is within hydrogen-bonding distance of R106, which would allow residues in loop 1 to bind the glutamine substrate. In the Release model, R106 is hydrogen bonding with the phosphate group of GMP (Fig. 7). It is plausible that R106 is functioning to help draw the product out of the nucleotide active site. Motion of loop 3 is also supported by the relatively high temperature factors reported in the crystal structure of the enzyme for this loop [2], which suggests high mobility for this segment [72]. Since they are connected via a hydrogen-bonding network, loop 3 may also induce a rearrangement in loop 2, bringing the latter into correct position for hydrogen bonding with glutamine and completing

Table 3
Residues in Triad Glutamine Amidotransferases Proposed to Function in Glutaminase Stimulus Signaling Across the Subdomain Interface.[a]

Enzyme	Organism	Catalytic triad	Proposed residues involved in signaling		
			Glutaminase	Acceptor domain	Acceptor active site
GMPS	*E. coli*	C86, H181, E183	H186	E383	K381
IGP synthase	*S. cerevisiae*	C83, H193, E195	K196	D359	T365
Anthranilate synthase	*S. solfataricus*	C84, H175, E177	H175	D275	D266
CTP synthetase	*E. coli*	C379, H515, E517	S520	H314	D303
FGAR-amidotransferase	*S. typhimurium*	C1135, H1260, E1262	R1263	R1263	E648

Carbamoyl phosphate synthetase is not included in this table because the interface in CPS includes an additional N-terminal domain that introduces an additional level of complexity into the domain interactions.

[a] A previous form of this table was published in [34].

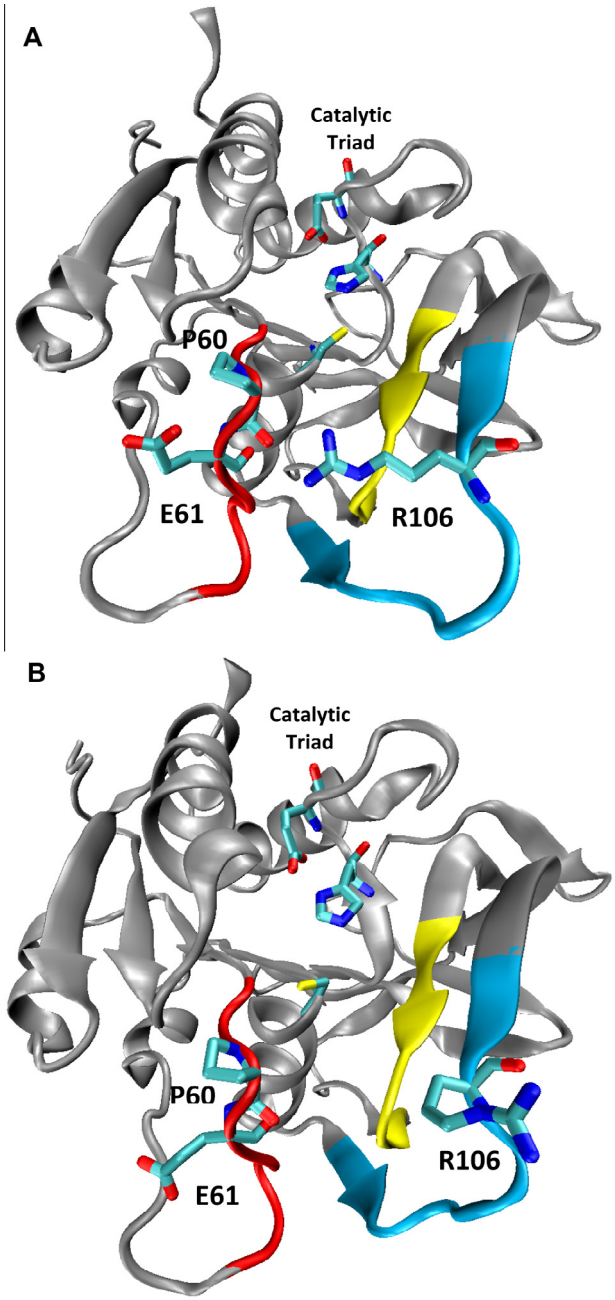

Fig. 6. Glutaminase domain indicating loops proposed to modulate glutaminase activity. (A) *E. coli* GMPS crystal structure 1gpm. (B) Catalytic model. Loop 1: residues 59–65 in red, Loop 2: residues 142–147 in yellow, Loop 3: residues 100–108 in blue. (For interpretation of the references to color in this figure legend, the reader is referred to the web version of this article.)

the binding site for the substrate. In this way, the conformational changes initiated by nucleotide substrate binding observed through tryptophan fluorescence analyses [38] may lead to the activation of the distal glutaminase active site by unblocking of the glutamine binding site.

Allosteric control in triad glutamine amidotransferases

The kinetic analyses described support the unified theory of triad glutamine amidotransferase allosteric control as being conferred in part through a conserved interdomain salt bridge. Direct contact between the two active sites in this family of proteins is achieved at the subdomain interface through ionic interactions between two highly conserved residues (Table 3). Disruption of these interactions results in diminished allostery. The results described here explain many of the features of GMPS that were unobtainable

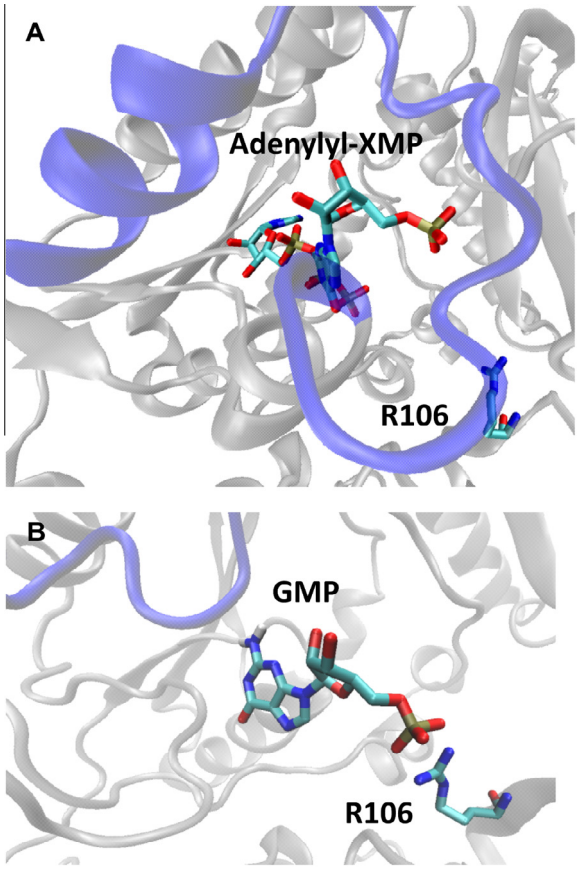

Fig. 7. (A) Catalytic model, showing R106 pointing towards intermediate (11 A away). (B) Release model, showing R106 hydrogen-bonding with GMP.

with crystallographic techniques. Biochemical data support a model of large-scale, substrate-induced conformational change that culminates in the fully active enzyme, capable of glutamine hydrolysis and intramolecular ammonia transfer.

Funding

The research was supported by grants from the National Institutes of Health [GM067195] (V.J.D), [P20RR016477] (R.S.L), [P20GM103434] (R.S.L), [T32GM008296] (J.C.O), and a National Science Foundation grant [NSF-IGERT 9987576] (J.C.O).

Notes

The authors declare no competing financial interests.

Acknowledgments

We would like to thank Shilpa Parakh, Larisa Avramova and Etti Harms for their contribution of the LIC expression constructs.

Appendix A. Supplementary data

Supplementary data associated with this article can be found, in the online version, at http://dx.doi.org/10.1016/j.abb.2014.01.004.

References

[1] H. Zalkin, Methods Enzymol. 113 (1985) 273–278.
[2] J.J. Tesmer, T.J. Klem, M.L. Deras, V.J. Davisson, J.L. Smith, Nat. Struct. Biol. 3 (1996) 74–86.
[3] H. Zalkin, J.L. Smith, Adv. Enzymol. Relat. Areas Mol. Biol. 72 (1998) 87–144.
[4] R.E. Amaro, R.S. Myers, V.J. Davisson, Z.A. Luthey-Schulten, Biophys. .J 89 (2005) 475–487.
[5] B.N. Chaudhuri, S.C. Lange, R.S. Myers, V.J. Davisson, J.L. Smith, Biochemistry 42 (2003) 7003–7012.
[6] F.M. Raushel, J.B. Thoden, H.M. Holden, Acc. Chem. Res. 36 (2003) 539–548.
[7] J.B. Thoden, S.G. Miran, J.C. Phillips, A.J. Howard, F.M. Raushel, H.M. Holden, Biochemistry 37 (1998) 8825–8831.
[8] T. Knochel, A. Ivens, G. Hester, A. Gonzalez, R. Bauerle, M. Wilmanns, K. Kirschner, J.N. Jansonius, Proc. Natl. Acad. Sci. USA 96 (1999) 9479–9484.
[9] B.N. Chaudhuri, S.C. Lange, R.S. Myers, S.V. Chittur, V.J. Davisson, J.L. Smith, Struct. (Camb.) 9 (2001) 987–997.
[10] J.A. Endrizzi, H. Kim, P.M. Anderson, E.P. Baldwin, Biochemistry 43 (2004) 6447–6463.
[11] R. Anand, A.A. Hoskins, J. Stubbe, S.E. Ealick, Biochemistry 43 (2004) 10328–10342.
[12] M. Strohmeier, T. Raschle, J. Mazurkiewicz, K. Rippe, I. Sinning, T.B. Fitzpatrick, I. Tews, Proc. Natl. Acad. Sci. USA 103 (2006) 19284–19289.
[13] L. Quemeneur, L.M. Gerland, M. Flacher, M. Ffrench, J.P. Revillard, L. Genestier, J. Immunol. 170 (2003) 4986–4995.
[14] L. Lou, J. Nakamura, S. Tsing, B. Nguyen, J. Chow, K. Straub, H. Chan, J. Barnett, Protein Expr. Purif. 6 (1995) 487–495.
[15] J. Nakamura, L. Lou, J. Biol. Chem. 270 (1995) 7347–7353.
[16] J.T. Ransom, Ther. Drug Monit. 17 (1995) 681–684.
[17] H. Karim, J. Hashemi, C. Larsson, A. Moshfegh, A.K. Fotoohi, F. Albertioni, Biochem. Biophys. Res. Commun. 411 (2011) 156–161.
[18] M. Kudo, Y. Saito, T. Sasaki, H. Akasaki, Y. Yamaguchi, M. Uehara, K. Fujikawa, M. Ishikawa, N. Hirasawa, M. Hiratsuka, Drug Metab. Pharmacokinet. 24 (2009) 557–564.
[19] A.C. Faesen, Mol. Cell 44 (2011) 147–159.
[20] S. Baba, M. Kanagawa, H. Yanai, T. Ishii, S. Kuramitsu, S. Yokoyama, G. Sampei, G. Kawai, (2007).
[21] S. Maruoka, S. Horita, W.C. Lee, K. Nagata, M. Tanokura, J. Mol. Biol. 395 (2010) 417–429.
[22] M.C. Franklin, J. Cheung, M. Rudolph, M. Cassidy, E. Gary, B.F.J. Love, Structure of the GMP synthase (guaA) from Coxiella burnetii (pdb: 3TQI), doi: 10.2210/pdb3tqi/pdb.
[23] A.K. Wernimont, A. Dong, T. Hills, M. Amani, A. Perieteanu, Y.H. Lin, P. Loppnau, C.H. Arrowsmith, A.M. Edwards, C. Bountra, J. Weigelt, R. Hui, (2011).
[24] M. Welin, L. Lehtio, A. Johansson, S. Flodin, T. Nyman, L. Tresaugues, M. Hammarstrom, S. Graslund, P. Nordlund, J. Mol. Biol. 423 (2013) 4323–4333.
[25] N. Sakamoto, G.W. Hatfield, H.S. Moyed, J. Biol. Chem. 247 (1972) 5880–5887.
[26] J.J.G. Tesmer, The crystal Structure Of A Paradigmatic Protein GMP Synthetase From *Escherichia coli* at 2.2 Angstroms Resolution Biology, Purdue University, West Lafayette, 1995.
[27] R. Ali, S. Kumar, H. Balaram, S. Sarma, Biochemistry 52 (2013) 4308–4323.
[28] A. Gutteridge, J. Thornton, FEBS Lett. 567 (2004) 67–73.
[29] J.M. Yon, D. Perahia, C. Ghelis, Biochimie 80 (1998) 33–42.
[30] J.Y. Bhat, R. Venkatachala, H. Balaram, FEBS J. 278 (2011) 3756–3768.
[31] J.M. Krahn, J.H. Kim, M.R. Burns, R.J. Parry, H. Zalkin, J.L. Smith, Biochemistry 36 (1997) 11061–11068.
[32] S. Chen, J.W. Burgner, J.M. Krahn, J.L. Smith, H. Zalkin, Biochemistry 38 (1999) 11659–11669.
[33] R.E. Amaro, A. Sethi, R.S. Myers, V.J. Davisson, Z.A. Luthey-Schulten, Biochemistry 46 (2007) 2156–2173.
[34] R.S. Myers, R.E. Amaro, Z.A. Luthey-Schulten, V.J. Davisson, Biochemistry 44 (2005) 11974–11985.
[35] I. Rivalta, M.M. Sultan, N.-S. Lee, G.A. Manley, J.P. Loria, V.S. Batista, Proc. Natl. Acad. Sci. USA 109 (2012) E1428–E1436.
[36] G.A. Manley, I. Rivalta, J.P. Loria, J. Phys. Chem. B 117 (2013) 3063–3073.
[37] F. List, M.C. Vega, A. Razeto, M.C. Hager, R. Sterner, M. Wilmanns, Chem. Biol. 19 (2012) 1589–1599.
[38] J.C. Oliver, R.S. Linger, S.V. Chittur, V.J. Davisson, Biochemistry 52 (2013) 5225–5235.
[39] T.T. Fukuyama, J. Biol. Chem. 241 (1966) 4745–4749.
[40] H. Zalkin, C.D. Truitt, J. Biol. Chem. 252 (1977) 5431–5436.
[41] J.Y. Bhat, R. Venkatachala, K. Singh, K. Gupta, S. Sarma, H. Balaram, Biochemistry 50 (2011) 3346–3356.
[42] N. Zyk, N. Citri, H.S. Moyed, Biochemistry 8 (1969) 2787–2794.
[43] J.J. Tesmer, T.L. Stemmler, J.E. Penner-Hahn, V.J. Davisson, J.L. Smith, Proteins 18 (1994) 394–403.
[44] U.K. Laemmli, Nature 227 (1970) 680–685.
[45] M. Abramoff, P. Magelhaes, S. Ram, Biophotonics Int. 11 (2004) 36–42.
[46] J.O. Pearcy, T.D. Lee, J. Am. Soc. Mass Spectrom. 12 (2001) 599–606.
[47] P. Schuck, Biophys. J. 78 (2000) 1606–1619.
[48] J. Garcia de la Torre, M.L. Huertas, B. Carrasco, Biophys. J. 78 (2000) 719–730.
[49] D.E. Kim, D. Chivian, D. Baker, Nucleic Acids Res. 32 (2004) W526–531.
[50] S. Crivelli, O. Kreylos, B. Hamann, N. Max, W. Bethel, J. Comput. Aided Mol. Des. 18 (2004) 271–285.
[51] G.J. Kleywegt, T.A. Jones, Acta Crystallogr. D Biol. Crystallogr. 50 (1994) 178–185.
[52] J. Liang, H. Edelsbrunner, C. Woodward, Protein Sci. 7 (1998) 1884–1897.
[53] J.D. Thompson, D.G. Higgins, T.J. Gibson, Nucleic Acids Res. 22 (1994) 4673–4680.
[54] T.A. Hall, Nucl. Acids. Symp. Ser. 41 (1999) 95–98.
[55] M. Landau, I. Mayrose, Y. Rosenberg, F. Glaser, E. Martz, T. Pupko, N. Ben-Tal, Nucleic Acids Res. 33 (2005) W299–302.
[56] S.F. Altschul, T.L. Madden, A.A. Schaffer, J. Zhang, Z. Zhang, W. Miller, D.J. Lipman, Nucleic Acids Res. 25 (1997) 3389–3402.
[57] M.L. Deras, S.V. Chittur, V.J. Davisson, Biochemistry 38 (1999) 303–310.
[58] R.S. Myers, J.R. Jensen, I.L. Deras, J.L. Smith, V.J. Davisson, Biochemistry 42 (2003) 7013–7022.
[59] N. Sakamoto, Methods Enzymol. LI (1978) 213–218.
[60] A. Fontana, P.P. de Laureto, B. Spolaore, E. Frare, P. Picotti, M. Zambonin, Acta Biochim. Pol. 51 (2004) 299–321.
[61] S.J. Hubbard, Biochim. Biophys. Acta 1382 (1998) 191–206.
[62] N. Errington, A.J. Rowe, Eur. Biophys. J. 32 (2003) 511–517.
[63] R. Ghirlando, A. Balbo, G. Piszczek, P.H. Brown, M.S. Lewis, C.A. Bratigam, P. Schuck, H. Zhao, Anal. Biochem. 440 (2013) 81–95.
[64] J.L. Smith, Curr. Opin. Struct. Biol. 8 (1998) 686–694.
[65] T.M. Larsen, S.K. Boehlein, S.M. Schuster, N.G. Richards, J.B. Thoden, H.M. Holden, I. Rayment, Biochemistry 38 (1999) 16146–16157.
[66] H.M. Holden, J.B. Thoden, F.M. Raushel, Curr. Opin. Struct. Biol. 8 (1998) 679–685.
[67] A. Teplyakov, G. Obmolova, B. Badet, M.A. Badet-Denisot, J. Mol. Biol. 313 (2001) 1093–1102.
[68] S. Mouilleron, B. Golinelli-Pimpaneau, Curr. Opin. Struct. Biol. 17 (2008) 653–664.
[69] A. Weeks, L. Lund, F.M. Raushel, Curr. Opin. Chem. Biol. 10 (2006) 465–472.
[70] X. Huang, H.M. Holden, F.M. Raushel, Annu. Rev. Biochem. 70 (2001) 149–180.
[71] A.-A. Li, D.V. Mavrodi, L.S. Thomashow, M. Roessle, W. Blankenfeldt, J. Biol. Chem. 286 (2011) 18213–18221.
[72] J. Drenth, Principles of Protein X-ray Crystallography, Springer-Verlag, New York, 1994.